 doi:10.20944/preprints202110.0418.v1

A comparative study on the mechanical properties and microstructure of cement-based materials by direct electric curing and steam curing

Zhihan Yang [a], Youjun Xie [a], Jionghuang He [a], Fan Wang [a], Xiaohui Zeng [a], Kunlin Ma [a], Guangcheng Long*[a]

[a] School of Civil Engineering, Central South University, Changsha 410075, Hunan, China

Abstract

Direct electric curing (EC) is a new green curing method for cement-based materials that improves the early mechanical properties via the uniform high temperature produced by Joule heating. To understand the effects of EC and steam curing (SC) on the mechanical properties and microstructure of cement-based materials, the mortar was cured at different temperature-controlled curing regimes (40°C, 60°C and 80°C). Meanwhile, mechanical properties, hydrate phase and pore structure of specimens were investigated. The energy consumption of two curing methods was compared and analyzed. The results show that the EC specimens have better and more stable growth of mechanical strength. The pore structure of EC specimen is also better than that of SC specimen at different maintenance ages. However, the hydration degree and products of samples cured by EC are similar to that SC samples. The energy consumption of EC is lower than SC. This study provides an important technical support for the EC in the production of energy-saving and high early-strength concrete precast components.

Keywords: Direct electric curing, Steam curing, Mechanical properties, Microstructure, Joule heat, Energy consumption

Introduction

Steam curing (SC) is a commonly used curing technology for cement concrete precast element production. The SC uses water vapor temperature to raise the environmental temperature, then accelerates the hydration process of cement-based materials [1,2], which promotes the growth of mechanical properties [3,4] and forms the morphology and characteristics of microstructure [5-8]. SC shortens the demolding times and to increases productivity, which improves the economic efficiency. However, many studies have suggested that SC has some adverse effects on specimens, such as coarsening of pores [9,10], thermal damage leading to cracking [11,12], reduction of long-term performance [13], and reduction of durability performance [14]. In response to the advantages and disadvantages of SC, a new direct electrical curing (EC) [15] method has been discovered by research scholars .EC uses fresh specimens with low resistivity [16] to generate uniform Joule heat under the current to accelerate the

Preprints (www.preprints.org) | NOT PEER-REVIEWED | Posted: 27 October 2021 doi:10.20944/preprints202110.0418.v1

hydration of cement and enhance early mechanical properties. Existing studies mentioned in the literature [17] include the feasibility of EC application [18,19], field application [20], electrodes arrangement [21], curing regime [22,23], effects of hydration process and microstructure [24,25], mineral admixtures [26], durability [16,27] etc. The current mainstream research direction mainly uses Joule heating to solve the problem of winter construction at ultra-low temperatures [28-31], repair and reinforcement of building structures [32], strengthening concrete [33-35]. These studies proved that EC has the following advantages: shortening the maintenance time, improving the early mechanical properties of cement, wide application prospects, low energy consumption, while the disadvantages also include thermal damage to specimens caused by high temperature, pore coarsening, and long-term performance degradation.

As a newly rapid curing method, there is little information related to the influence of EC on properties and structures cementitious materials, has been less studied on cement-based materials than SC, especially there is no comparative study on the effect on cement mortar. In order to understand the effects of SC and EC on cement-based materials under the same curing regime, this paper investigates the effects of SC and EC on the mechanical properties and microstructure of cement mortar, with special attention to the corresponding mechanisms and energy consumption. This research aims at providing some technical support for the production of low-energy and early high-strength precast components by application EC method.

2 Materials and experiments

2.1 Materials and Equipment

The cement used in this experiment is Reference Portland cement with strength grade of 42.5MPa produced by China United Cement Group, Ltd. The chemical composition of cement is shown in Tab.1. The sand used is river sand with a grain size of 2.8 mm.The cement mortar mold with a size of 40mm× 40mm× 160mm was used in this experiment.

Table 1. Chemical compositions of cement and mineral composition (wt%).

SiO_2	Al_2O_3	Fe_2O_3	CaO	MgO	SO_3	LOI	C_3S	C_2S	C_3A	C_4AF
20.58	5.03	3.38	63.32	2.01	2.06	1.76	57.55	17.82	7.54	11.19

The equipment used and the arrangement are shown in Figure 1(a). The homemade insulation box and alternative current (AC) power supply was used to cure the EC specimens. The insulation box is composed of an external sealed plastic box and an internal aluminum foil sponge patch. The AC power supply model (IVYTECH, APS-4000C) has a voltage range from 0V to 300V and a frequency range from 45Hz to 250Hz. High-precision anti-interference temperature sensors (WZP-PT100) and AC transducers (SIN-SDJI-B-500mA) were employed to detect the temperature and current of the specimens. The tested date was input to the multi-channel paperless recorder (Sinomeasure, SIN-R6000F) for recording. In addition, graphite electrodes and silver-plated wires were used in this study to guarantee high electrical conductivity and

Preprints (www.preprints.org) | NOT PEER-REVIEWED | Posted: 27 October 2021 doi:10.20944/preprints202110.0418.v1

stability. It is noted that they do not react with the cement paste, which avoids the change of hydrate phase and reduce losses of energy during current transmission. The schematic diagram of the specimen during the curing regime is shown in Figure 1(b). The water bath tank provided a curing space with 600mm×300mm×200mm for SC specimens and it's heating power is 2000w.

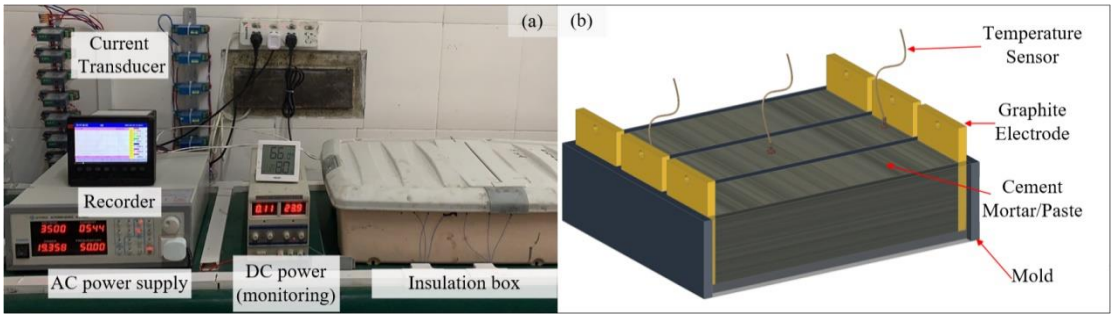

Figure 1. The equipment for EC (a) and the diagram of the specimens (b).

2.2 Experimental methods

In this study, the cement mortar was prepared test the strength development and the macropore characteristics. Meanwhile, the cement pastes were used to explore the hydration degree, hydration products and microstructure.

2.2.1 Casting and curing

In casting and curing, two graphite electrodes with a size of 40 mm × 50 mm × 5 mm were placed on both ends of the molds and fixed with hot melt adhesive. The mass ratio of cement to sand for mortar sample is 1:2, and the water-cement ratio is 0.35. The cement and sand were put in a mortar mixing pot and stirred for 1 minute to make it evenly mixed. After adding the water, the mixing regime included slow mixing (150r/min) for 2minutes and fast mixing (300r/min) for 2 minutes. After mixing, the cement mortar was poured into the molds and then a vibrating table was used for compacting the mortar with two 5-second compaction sessions. The polyethylene film was used to seal the surface of the specimens to prevent water evaporation after vibrating. Before the start of the curing regime, the EC and SC specimens were put into the homemade insulation box and water bath tank, respectively, and the temperature sensor was inserted into the positive center of the specimen.

The curing regime was divided into four stages as shown in Fig.2, including waiting period (0-1 hour), heating period (1-3 hour), thermostatic period (3-11 hour) and cooling period (11-13 hour). The temperature rise rate of the three curing regimes were 10, 20, 30℃/h, and the temperature in the constant temperature stage was 40,60,80℃ respectively. The EC specimen started to be applied voltage in the heating period, when entering the constant temperature period, the cement paste was only applied 0.5V to reduce the Joule heat due to the hydration heat release. Then the applied voltage had to raise to increase the Joule heat to keep the temperature of the specimens due to the hydration heat was reduced. At the end of 11 hours of curing, the specimens were cool down in a controlled manner after the AC power was turned off. The same curing regime was also used in the SC, and the different place was the SC specimens were controlled by the water vapor temperature in the water bath tank. In this paper, three

Preprints (www.preprints.org) | NOT PEER-REVIEWED | Posted: 27 October 2021 doi:10.20944/preprints202110.0418.v1

curing regimes (40℃,60℃,80℃) were selected and three groups of specimens with different curing methods were formed, and the specific specimen parameters are shown in Tab. 2.

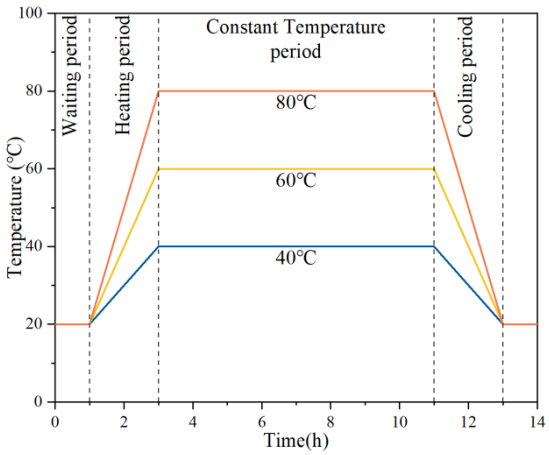

Figure 2. The curing regimes on this experiment.

Table 2. The parameters of different curing methods for specimens.

Group	Curing method	Curing regime(℃)	Cement pasts
SC40	Steam	40	-
SC60	Steam	60	Casted and cured
SC80	Steam	80	-
EC40	Electric	40	-
EC60	Electric	60	Casted and cured
EC80	Electric	80	-
NC	Normal	20	Casted and cured

2.2.2 Testing

The specimens were demolded immediately after the curing regime and then put into the standard curing room (20±2℃; 95±5% RH). The specimens were taken out from the standard curing room at the corresponding curing age and left to dry naturally for 2 hours before the compressive and flexural strength test. The broken samples were left for microscopic testing. Three specimens were tested the flexural strength, and then six broken specimens were used to test compressive strength test. The loading rate was kept at 50N/s during flexural strength tests and 2.4kN/s during compressive strength. The average of strength of three specimens was used as the representative strength value. After mechanical tests, the suitable samples were selected for the hydration process and microstructure test, including Thermogravimetric analysis (TGA), X-ray diffraction analysis (XRD), Scanning Electron microscope (SEM), Mercury Intrusion Porosimetry (MIP), and Macro/meso-scopic Pore Image Analysis (MIA) measurements.

The hydration degree and hydration products were tested by TGA and XRD. TGA samples (approximately 50mg) were tested from room temperature to 950℃ at a heating rate of 10℃/min under a N_2 atmosphere by equipment of TGA 2(SF)-Mettler Toledo. The weight loss of samples was calculated the chemical bound ware (RT-550℃) and portlandite (400℃-550℃).

The pore structure of cement paste samples were tested by MIP and MIA. MIP samples with length 20mm and diameter 12mm obtained by cement pastes were immersed in the isopropanol for 7 days and vacuum-drying for 7 days, and then tested

Preprints (www.preprints.org) | NOT PEER-REVIEWED | Posted: 27 October 2021 doi:10.20944/preprints202110.0418.v1

by equipment of Micrometrics Autopore IV-9500. The MIP machine was set to equilibrate for 10 s at each pressure point. The contact angle was 130° and surface tension was 0.485 N/m. MIA measurement was conducted by taking photos of different locations on the surface of the specimen using microscope magnification, identifying the air holes in the photos by software, and calculating the size and area of the air holes in the specimen using C++ programming language. Three cement mortar specimens were split in the middle of the length direction by cutting machine. The cut pieces were selected as the observation surface, and were ground smooth by the grinder in three times. The specimens were ground for 800, 100 and 1200 meshes using silicon carbide powders. Then the black marker was used to black out the observation surface of the specimens. After the surface was dry, the heated zinc oxide-Vaseline pastes were poured on the surface to let it flow into the pores in the observation surface. After cooling down to the room temperature, the excess pastes were scratch off with a scraper. Six specimens were put down under the microscope camera for clear observation. The white pixels in the image were automatically recognized as aperture by the computer.

Two hundred and twenty-five microscopic images were captured for each observation surface by scanning along X and Y axis fifteen times respectively, starting from the upper left corner of sample. The porosity and pore diameter distribution were, then, automatically calculated through an algorithm realized by C++ programming language according to the following equations:

$$A_i = \sum_{j=1}^{m_i} A_j \tag{1}$$

$$D_j = \sqrt{\frac{4A_j}{\pi}} \tag{2}$$

$$A\% = \frac{\sum_{i=1}^{15} A_i}{225 A_T} \tag{3}$$

where A_i is the total pore area in the i_{th} microscopic image; A_j the area of one certain pore; D_j the equivalent diameter of the corresponding pore; A_T the area of each microscopic image and $A\%$ the total pore area ratio of the specimen observed. For each analysis, the test surface is to analyze three times starting in a different corner of the sample. By testing 18 analyses of six specimens, the average value of those measurements is adopted.

The morphology of hydration product in cement paste sample was scanned by the JSM-IT500LV instrument (JEOL Ltd. Microscopy) under an accelerating voltage ranging from 10kV to 20kV. The selected samples should have a flat and polished surface.

3 Results and discussion

3.1 Strength development

Fig.3 shows the strength development of the specimens in SC and EC. There are several parts worth noting. Firstly, except for the SC80, the strength of SC and EC specimens steady increased with curing time. Secondly, the higher curing temperature,

Preprints (www.preprints.org) | NOT PEER-REVIEWED | Posted: 27 October 2021 doi:10.20944/preprints202110.0418.v1

the lower the strength growth rate of specimens at 28 and 56 days. Compared with NC specimens, the strength of SC and EC specimens at 1 and 3 days was better, but the strength of some specimens became lower in 7, 28 and 56 days. Finally, the strength of EC specimens was better than that of SC specimens under the same curing temperature and age.

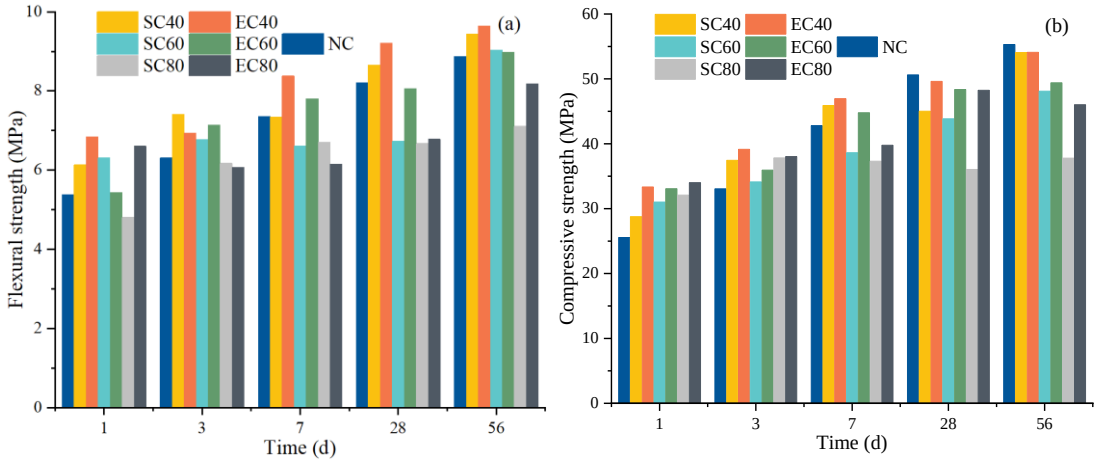

Figure 3. The strength development of specimens under different curing conditions

The variation of flexural strength of the specimen was basically the same as that of compressive strength. The 1-day compressive strength of NC specimens reached 46.22% of the 56-day NC specimens. All 1-day SC and EC specimens improved by 12.55%-33.02% compared to NC-1d，and reached 52.02%-61.48% of NC-56d compressive strength. It implied that SC and EC could greatly improve the early strength of cement mortar. With the increase of age, the mechanical properties of all groups except SC80 of specimens were improved. Compared to NC specimens, the compressive strength of EC40 was increased by 30.45% (1 day), 18.46% (3 days), 9.7% (7 days), minus 1.98% (28 days) and minus 2.17% (56 days). While SC40 is only 12.55% (1 day), 13.31% (3 days), 7.24% (7 days), minus 11.06% (28 days), minus 2.24% (56 days). The mechanical strength results from other curing regimes showed that EC specimens could achieve better mechanical properties than SC specimens. This result indicates that the EC method is a good rapid curing method, which is more conducive to strength development of sample compared to steam curing condition.

3.2 Hydration degree and products

There is a close relationship between mechanical properties and hydration process and products of cement concrete. Since cement mortar contains sand, which affects the microscopic test results, TG and XRD tests were performed on cement pastes cured under the same regime to analyze the corresponding hydration characteristics in this paper. Samples of different ages under 60°C Curing regime were selected for test the hydration degree and hydration products. The reason for this choice is due to that the 60℃is the recommended curing regime in the steam curing methods[36,37].

For the hydration degree analysis, samples with different maintenance ages were selected for TG tests and the results were shown in Fig.4. The TG and DTG curves

Preprints (www.preprints.org) | NOT PEER-REVIEWED | Posted: 27 October 2021 doi:10.20944/preprints202110.0418.v1

showed standard cement curves for specimens. where the two groups of specimens are slightly different at the same age. Based on the results shown in Fig.4, the hydration products and the degree of hydration were listed in Tab.3.

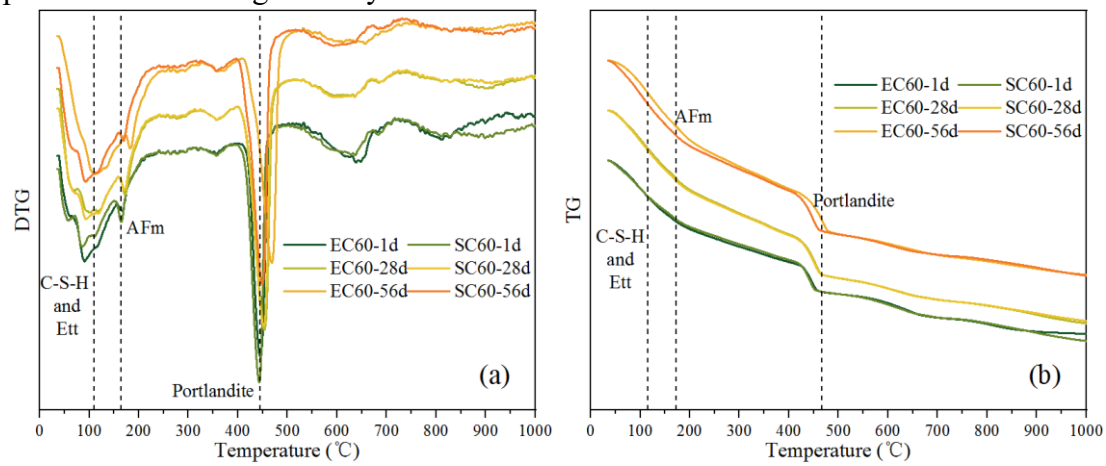

Figure 4. The TG/DTG results of samples at different ages.

Table 3. The hydration products and degree of samples obtained by TG test (%)

	SC60-1d	EC60-1d	SC60-28d	EC60-28d	SC60-56d	EC60-56d
Portlandite	18.23	17.16	23.91	24.43	24.59	25.57
Chemically-bound water	13.77	13.71	17.21	17.23	17.85	17.82
Hydration degree	71.66	67.49	88.17	90.51	89.42	94.44

The values of SC samples in the Portlandite data were larger than EC at 1 day, and slightly smaller at 28 and 56 days. This could be caused by the higher temperature in the SC specimens compared to the EC during the curing regime, thus promoting the hydration of the cement faster, as will be discussed in 3.4.1. Chemically-bound water data showed that both curing methods promoted the dissolution and hydration of cement particles to the same extent. Hydration degree was calculated by equation 4. It can be found that the two curing methods have reached 71.66-67.49% hydration degree at 1 day, which indicates that the two curing methods can accelerate the hydration of cement and quickly improve the early mechanical properties of cement mortar. Both the SC and EC specimens at 28 and 56 days were able to achieve more than 86% of the hydration degree, especially the EC60 at 56 days reached 94.44%, which indicated that besides accelerating the hydration of the cement, two curing methods kept a continuous increasing in the mechanical properties of the cement mortar.

$$\alpha = \frac{W_n}{n} - LOI \tag{4}$$

In the hydration products testing section, XRD was used to test the type and quantity of hydration products of SC and EC samples, and the test results were shown in Fig.5. The XRD curves showed standard cement hydration products formed in the samples of SC and EC, which indicated that no new hydration products were formed in EC specimens under the influence of current.

Tab.4 demonstrated the quantities of each physical phase in cement pastes by quantitatively analyzing the XRD data. Fig.6 demonstrated the distribution of the physical phases, which showed the ratio of cement hydration products and cement

Preprints (www.preprints.org) | NOT PEER-REVIEWED | Posted: 27 October 2021 doi:10.20944/preprints202110.0418.v1

minerals in the specimens. SC and EC improved the early strength of the specimens by promoting the dissolution of the four main cement minerals. The results of the 1-day test showed that the remaining amount of C_3S in the EC specimen was less than that of SC, but more C_2S than SC, which indicated that EC increased the hydration of cement by promoting the dissolution of C_3S and inhibiting the dissolution of C_2S, a situation that is the same as that in the literature[17].In the subsequent standard maintenance, the specimens consumed cement minerals by natural hydration, therefore the four cement minerals were the same in the SC and EC specimens at 28 and 56 days. Portlandite and Amorphous generated in specimens were also essentially the same, indicating that SC and EC have the same promotion effect on the production of cement hydration products. and this was consistent with the results of TG.

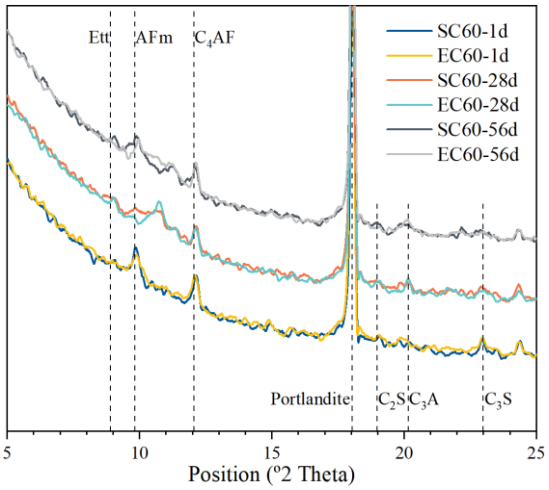

Figure 5. XRD analysis curve of specimens under different curing regimes.

Table 4. Phase proportion calculated by XRD data (%)

	C_3S	C_2S	C_3A	C_4AF	Portlandite	Amorphous
SC60-1d	18.95	11.78	1.99	7.17	17.77	41.99
EC60-1d	16.87	14.74	2.00	7.15	17.07	42.17
SC60-28d	11.27	12.62	0.46	5.59	22.21	47.54
EC60-28d	11.69	11.96	0.92	5.17	22.56	47.70
SC60-56d	9.56	9.39	1.23	5.14	24.56	49.96
EC60-56d	9.81	9.65	0.61	5.57	24.56	49.80

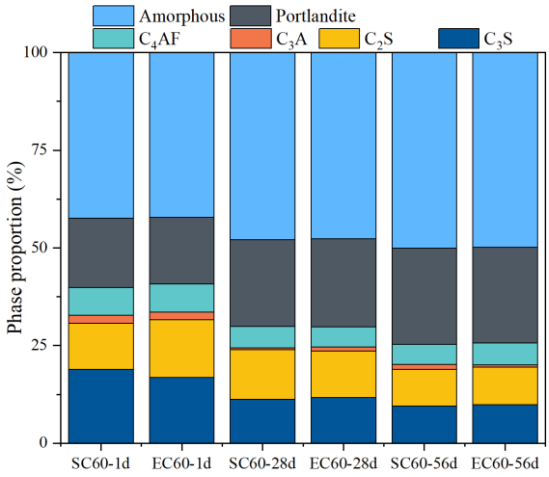

Figure 6. Phase proportion of specimens under different curing regimes.

Preprints (www.preprints.org) | NOT PEER-REVIEWED | Posted: 27 October 2021 doi:10.20944/preprints202110.0418.v1

3.3 Pore structure

3.3.1 Microscopic pore structure

To explain the differences in the mechanical properties of the specimens, the analysis of pore structure was further analyzed.

The pore structure of the specimens at different ages under different curing methods was tested by MIP, and the test results are shown in Fig.7. It showed that the number of pores in the range of 20-50nm gradually decreased for both specimens as the age increased, while the number of pores below 20 nm was gradually increasing. This indicated that with the growth of the age, the specimen was continuously hydrated, refining the original existence of pores. In addition, the EC60 had more pores with the sizes between 10-50 nm than SC60 and fewer pores near 100 nm. Unlike the effect of SC coarsening the pores of cement paste[9,10], EC makes the pore size of cement paste smaller and increases the number of small pores. The data analysis was plotted in Tab.5.

The Porosity results (Tab.5) indicated that the difference between EC and SC specimens at the same age was not significant, but the Probable pore size results showed that the pore size of EC specimens was smaller. This indicated that the pore size inside the EC specimen was smaller than that of the SC specimen for the same porosity. The pores in the cement paste can be divided into four types according to the pore diameters [38]: large pores ($d \geq 1000nm$), capillary pores ($1000nm \leq d < 100nm$), transition pores ($10nm \leq d < 100nm$), and gel pores ($d < 10nm$). Among them, pores greater than 100 nm in diameter are harmful pores, leading to a decrease in mortar strength [39]. The pores distribution data in Tab. 5 were plotted by pore type in Fig. 8. The figure indicated that the number of gel pores of the specimens slightly increased with increasing age. The number of transition pores decreased by filling with dense hydration products. The number of pores above 100 nm was higher for SC60 than for EC60, which indicates that SC caused the coarsening of pores and the formation of more harmful pores, thus affecting the strength development of the specimens.

Preprints (www.preprints.org) | NOT PEER-REVIEWED | Posted: 27 October 2021 doi:10.20944/preprints202110.0418.v1

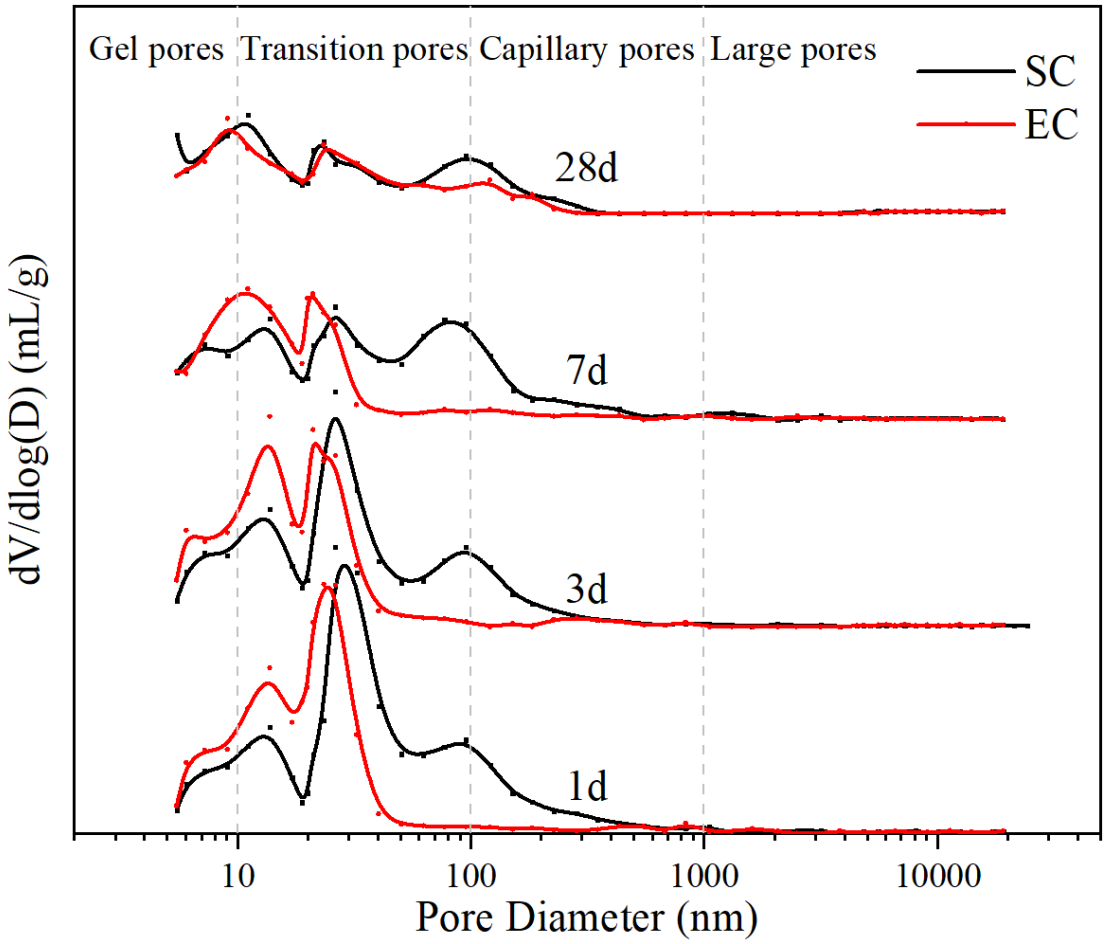

Figure 7. Pore size distribution of SC60 and EC60 specimens at different ages.

Table 5. The pore characteristics of specimens under different curing regimes.

Specimen No.		SC60 -1d	EC60 -1d	SC60 -3d	EC60 -3d	SC60 -7d	EC60 -7d	SC60 -28d	EC60 -28d
Porosity/%		18.37	17.26	15.92	15.83	14.34	12.21	8.96	8.61
Probable pore size /nm		26.30	23.41	26.30	21.10	13.74	11.06	11.06	9.06
Pores distribution/%	<10nm	1.53	2.02	1.75	2.53	1.99	3.78	2.38	1.70
	10-100nm	13.67	14.38	11.79	12.71	9.45	8.23	4.84	5.81
	100-1000nm	2.77	0.52	2.11	0.39	2.46	0.50	1.54	0.88
	>1000nm	0.39	0.35	0.27	0.21	0.06	0.30	0.20	0.22

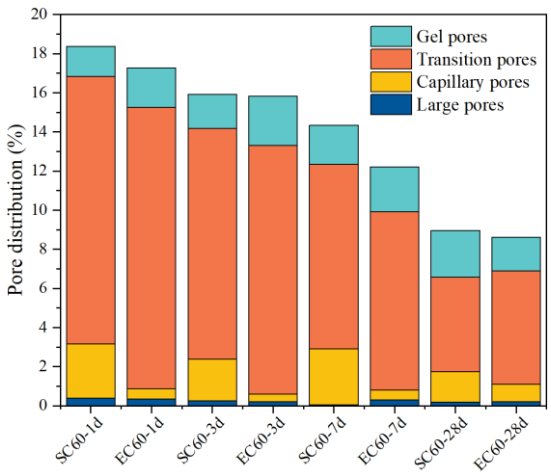

Preprints (www.preprints.org) | NOT PEER-REVIEWED | Posted: 27 October 2021 doi:10.20944/preprints202110.0418.v1

Figure 8. Stacked histogram of pore size distribution of specimens under different curing methods.

The MIP results showed the difference between the pore structures of SC and EC specimens. The porosity of two samples were both decreasing with increasing age, which means that the pores formed in the early rapid curing regime of the samples will continue to hydrate and fill densely under standard maintenance. In addition, SC samples had larger porosity than EC samples, which may be due to the uneven temperature control of the specimens in the curing regime. Uneven high temperature curing led to the formation of temperature gradients inside the sample, and different cement compositions and hydration products produced different expansions, leading to more pore generation. In terms of the most probable pore size, the pore size with the highest pores' number in SC was larger than that in EC, indicating that the distribution of pore sizes was affected by different curing methods. Finally, SC samples formed more harmful pores (>100 nm) than EC samples, which explained the poorer mechanical properties of SC samples than EC samples. In addition, the gel pores and transition pores of SC samples were less than EC, which means that a more porous pore structure was formed with the same porosity. Therefore, MIP results indicated that EC is a better curing method than SC, resulting in a better pore structure inside the cement specimens.

3.3.2 Macro/mesoscopic Pore Image Analysis

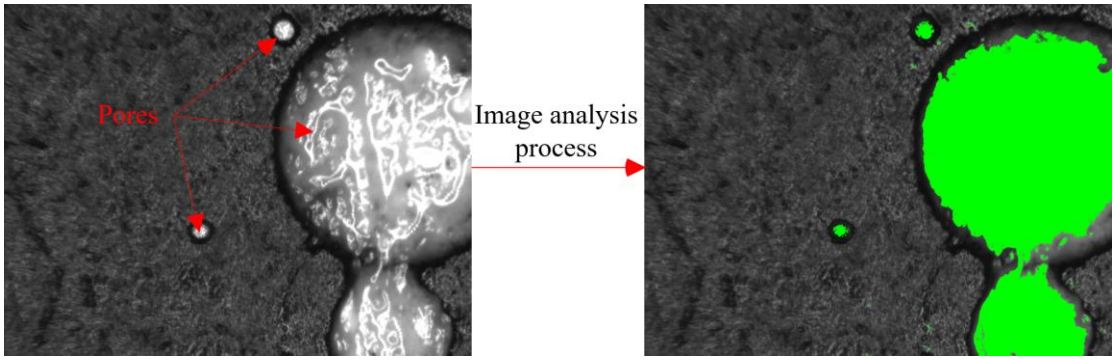

Figure 9. Schematic diagram of MIA method.

Preprints (www.preprints.org) | NOT PEER-REVIEWED | Posted: 27 October 2021 doi:10.20944/preprints202110.0418.v1

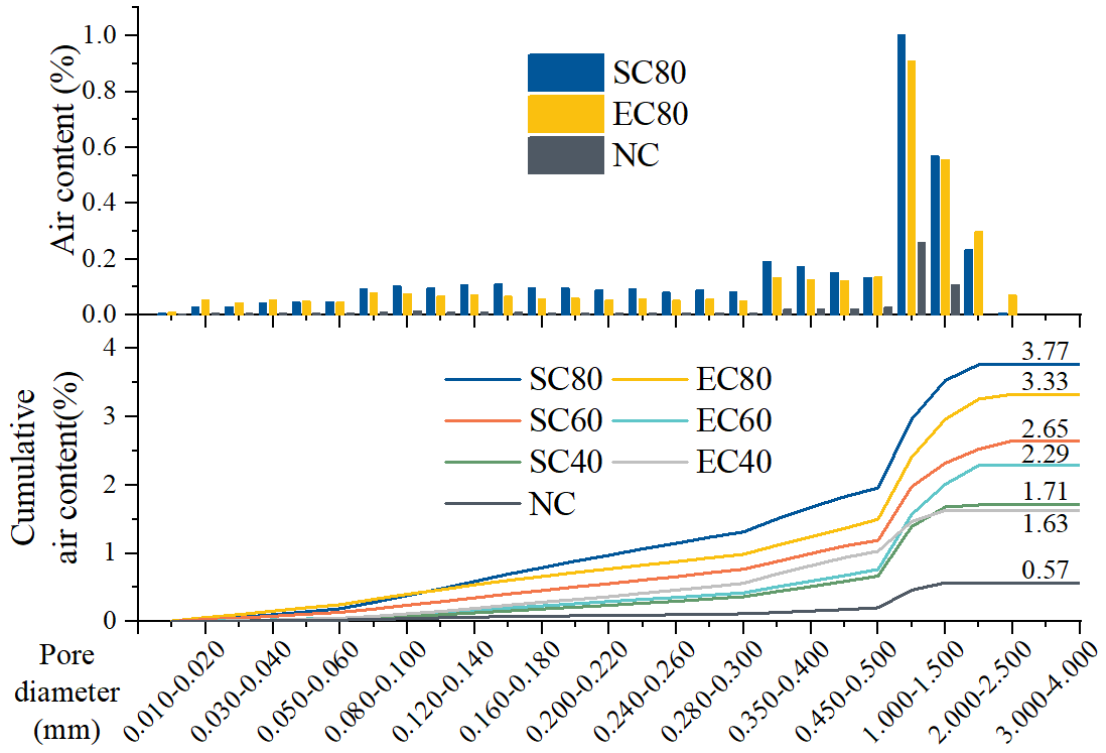

Figure 10. The pore size distribution of 28-day specimens.

Air voids in hardened concrete which result from the using of superplasticizer and the inevitably introducing of air during mixing are usually larger than 2 μm. The air void structure of hardened specimens under different curing methods at 28-day can be observed by using microscopic camera. As seen from Fig.9, the air voids on the specimen surface were identified by MIA and marked as green part by the software. The air distribution and cumulative air content of the 28-day specimens were obtained by calculating the area and size of the green part in all photos by equation (1-3), and the calculation results were shown in Fig.10. For the convenience of observation, the distribution of the number of pores was expressed using only three groups of specimens, SC80, EC80 and NC. The number of air voids in EC80 specimens with different pore sizes was smaller than that in SC80 specimens. And between 0.5 to 2.5 mm air voids sizes, SC and EC specimens showed a large number of pores compared to NC specimens. The cumulative air content within 0.5mm of the air voids size of SC and EC specimens increased by 0.09% and 0.02%, respectively, compared to the NC specimens. However, the cumulative air content within 2.5mm air voids size of SC and EC specimens increased by 2.08% and 1.72% compared to the 0.57% of NC specimen. These data demonstrated that the SC and EC specimens had more air voids inside the specimens than NC, which would reduce the strength of the specimens. Also, the SC specimens had more air voids than the EC specimens, which also meant that the strength of SC specimens would reduce. The MIA results matched the mechanical properties results.

The pore evolution of SC and EC specimens at the microscopic scale and the distribution of air voids at the macroscopic scale were obtained by testing MIP and MIA. The pore structure of EC sample was more refined on the microscopic scale than that in SC, the formation of gel pores and transition pores was promoted, and the generation

Preprints (www.preprints.org) | NOT PEER-REVIEWED | Posted: 27 October 2021 doi:10.20944/preprints202110.0418.v1

of capillary pores was reduced. On the macroscopic scale, EC specimens produced more air voids than NC specimens but less than SC specimens. The pore structure data results matched the mechanical property results, which indicated that the EC specimens had better pore structure than the SC specimens.

3.4 Discussion

The above results demonstrated that SC and EC accelerated the dissolution of cement minerals in the specimens at the early stage, promoted the formation of portlandites, accelerated the hydration of cement, and enhanced the early mechanical properties of the specimens. The study of pore structure indicated that the pore structure of SC and EC was the main reason for the influence of mechanical properties. To understand the formation of pore structure, temperature evolution of specimens in different curing regimes were used to analyze the heat flow transfer characteristic and effect of SC and EC. Finally, the energy consumption of the two curing methods was discussed.

3.4.1 Temperature evolution during curing regimes

The temperature evolution under different curing regimes was recorded in Fig. 11. The internal temperature of the SC specimens showed to be lower than the EC specimens during the heating period and higher than the EC specimens in the early part of the constant temperature period.

The SC specimens were heating by the thermal radiation of the water vapor temperature in the water bath tank. The water vapor temperature must increase in order to raise the temperature of specimen. During the heating period, the SC specimen generated a temperature gradient inside the specimen due to the increasing water vapor temperature and the inefficiency of thermal radiation, which is the main reason for the thermal damage of the specimens. The temperature of EC specimen was controlled by adjusting the voltage during the heating stage. When the EC specimen temperature was lower or higher than the curing regime temperature, the voltage was increased or decreased to the Joule heat inside the specimen.

In the constant temperature period, the SC specimen was affected by the water vapor temperature and its own exothermic hydration, which caused the specimens temperature to exceed the control temperature. EC controlled the temperature of specimens by Joule heat and there was no overheating occurred. It was necessary to mention that the temperature of the EC specimen fluctuated during the constant temperature period, which was caused by the manual voltage adjustment and could be avoided by the subsequent development of the equipment.

In the cooling period, specimens cooled down quickly and reached room temperature by opening the box lid for heat dissipation. Since the water bath tank and the insulation box had certain thermal insulation capacity, the temperature of the two specimens was higher than that of the standard NC specimen after the cooling period.

The results indicated that EC was better than SC for the control of specimen temperature. The mechanical properties of SC and EC specimens were different in the early age, the result might be the uncontrolled temperature in the specimens during the constant temperature period. SC is a curing method using thermal radiation to heat the

Preprints (www.preprints.org) | NOT PEER-REVIEWED | Posted: 27 October 2021 doi:10.20944/preprints202110.0418.v1

specimens, in other words, it suffers the limitations of being a surface-heating method and it will cause a temperature gradient inside the specimens. EC is a volume-heating method by using the Joule heat produced in the specimens to heat specimens. In the first 3 hours, the environment temperature had reached 40/60/80℃, but with the hydration exothermic action, the inner temperature of SC specimen was rising and became uncontrolled. Although EC specimen has this situation, it is easier to control the temperature by adjust the applied voltage. Therefore, the possible reason to explain the different results of mechanical properties in early age was that the temperature of SC specimens in the curing regime was higher than that in EC. For the 28-day and 56-day specimens, the mechanical properties of EC60 were higher than those of SC60. It is because that the EC reduced the microstructural damage during the curing regime, and the unhydrated cement particles in the specimens were better hydrated than those in the SC specimens in the standard maintenance.

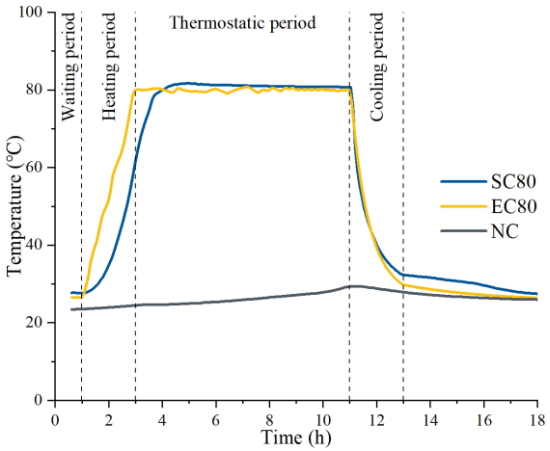

Figure 11. Evolution of temperatures during different curing regimes.

3.4.2 The heat flow transfer characteristics of two curing methods

The heating principle and heat flow transfer of the two curing methods was analyzed and shown in Fig.12.

The SC specimen was heated up by heat radiation from water vapor temperature in the water bath tank. The thermal energy first transmitted to the specimen surface and then to its interior, thus forming a multi-level temperature gradient in the SC specimens. While the EC specimen was heated up by Joule heat through the flow of AC in the interior of the specimen, using the cement paste with low resistance in the early hydration process. The difference in heat transmission between SC and EC leads to a different heat flow transfer characteristic. For example, the temperature control capability of SC and EC is different. the temperature control capability of SC is mainly determined by the heat transfer efficiency. Cement and concrete are poor conductor of heat transfer and has defects for thermal transfer. The temperature control ability of EC is mainly determined by the resistivity of the cement-based material. The low resistivity of fresh pastes and the adjustable voltage constitute an excellent control capability. Meanwhile, SC is a surface-heating method and EC is a volume-heating method. The direction of heat transfer determines the temperature gradient inside the specimen. From the surface to the interior of the SC specimens, the temperature transfer forms a multi-layer temperature gradient, resulting in defects caused by different temperature

Preprints (www.preprints.org) | NOT PEER-REVIEWED | Posted: 27 October 2021 doi:10.20944/preprints202110.0418.v1

expansion of the material. EC specimens generate heat internally, which specimens undergo an overall heating by Joule heat, reducing the effect of temperature gradient. In addition, the curing efficiency of SC is poorer than that of EC. From the perspective of energy conversion, SC is an indirect curing method by converting water vapor temperature to specimen temperature. While EC is a direct and fast curing method by heating the whole specimen through Joule heat.

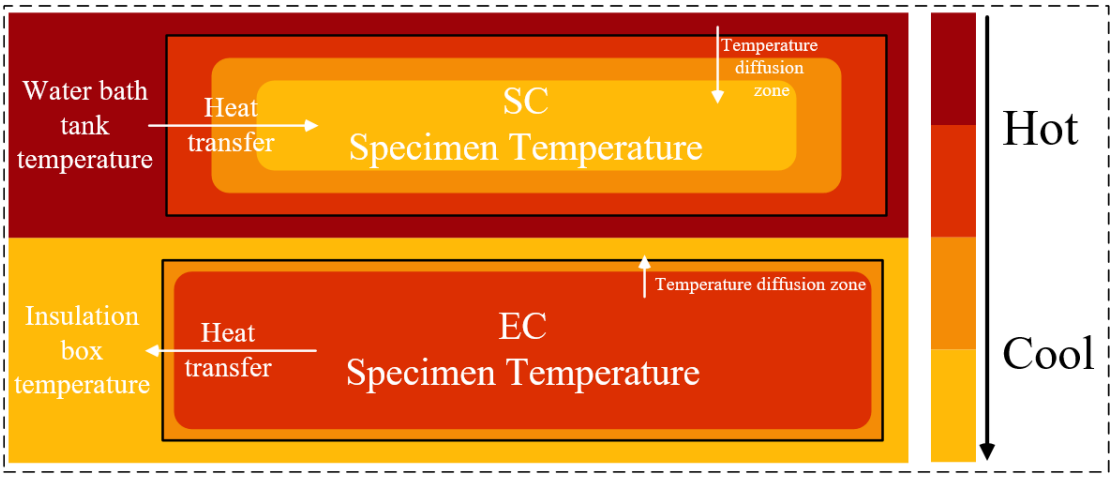

Figure 12. Temperature distribution of specimens under two curing methods.

After explaining the heat flow transfer characteristic of the two curing methods, SEM was used to observe the specimens cured by the two curing methods, and thus the morphology of the hydration products was analyzed.

Fig.13 demonstrated the overall morphology of the microstructure by magnifying the hydration product at 1000×, and it can be found that the EC sample of 1-day promoted the dense hydration product with some pores, while the SC sample had more loose hydration products on this basis. In the test of 28-day sample, the morphology of hydration phases of NC and EC samples was shown, and it can be found that the samples were dense, only that the EC sample had more pores.

Preprints (www.preprints.org) | NOT PEER-REVIEWED | Posted: 27 October 2021 doi:10.20944/preprints202110.0418.v1

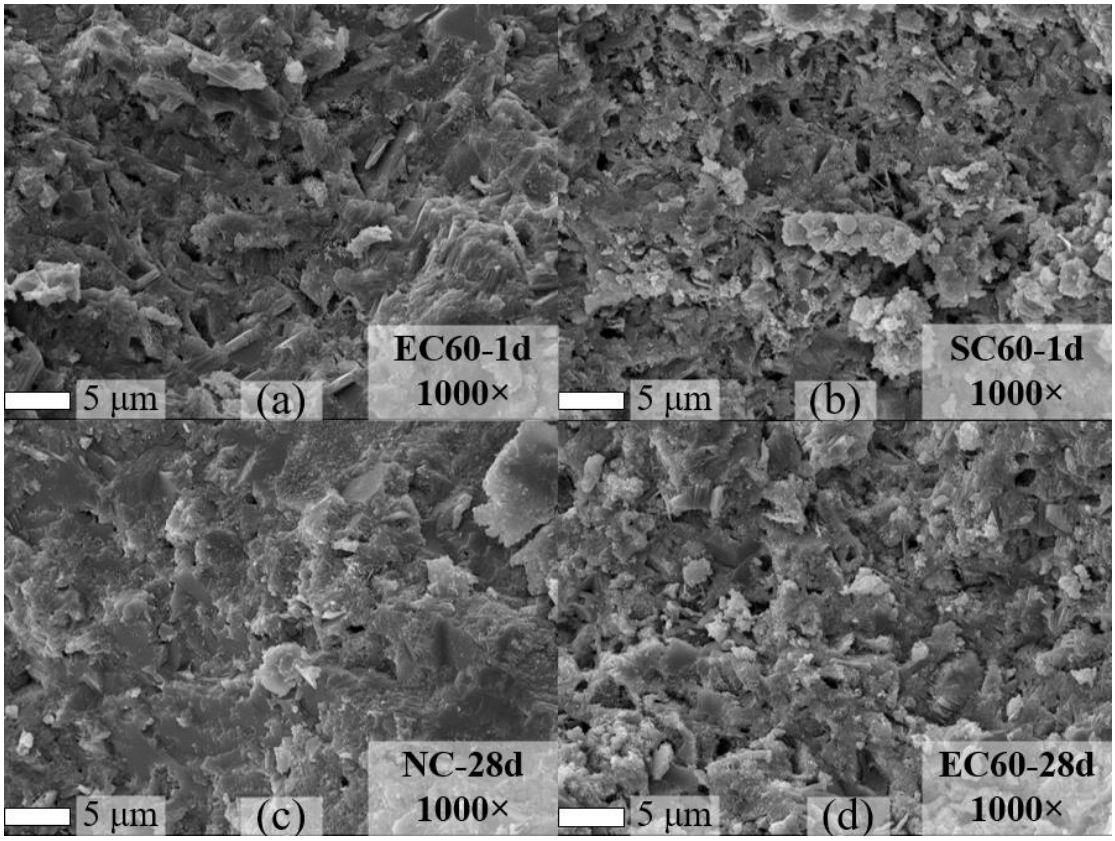

Figure 13. The 1000× SEM picture of specimens

SEM at 5000× was used to observe the microscopic hydration products of the samples (Fig.14). The 1-day SC sample exhibited a coarser C-S-H morphology and pore structure than EC. The loose C-S-H gels in the SC sample contained a large number of voids, resulting in reduced stability of the cement-based material connections, while the C-S-H in the EC samples grew attached to the dense hydration products and needle-like AFt grew in the pores to enhance the connection. For 28 days, the test results showed that the EC60-28d samples formed pores with C-S-H gel growth compared to the hydrated compactness of NC-28d.

As observed by SEM, the two curing methods caused different effects on the hydration products inside the specimens through different heat flow transfer characteristic. Because of temperature gradient and high temperature, SC specimens formed more pores present in the hydrated phase morphology, although there was the generation of C-S-H gel, but the connection of hydration products in the pores was not tight as EC specimens. In addition, the microscopic morphology of EC-28d was similar to that of NC-28d specimens, and even though pores existed in EC specimens, the internal C-S-H gels interconnected to enhance the connection. For SC and EC specimens, the high temperature accelerated the cement hydration and dense the early hydration products, but also generated pores. Due to more uniform and effective temperature control, EC specimens were better connected on the hydrated phase than SC, which explains the better connection of EC than SC in the 28-day strength test.

Preprints (www.preprints.org) | NOT PEER-REVIEWED | Posted: 27 October 2021 doi:10.20944/preprints202110.0418.v1

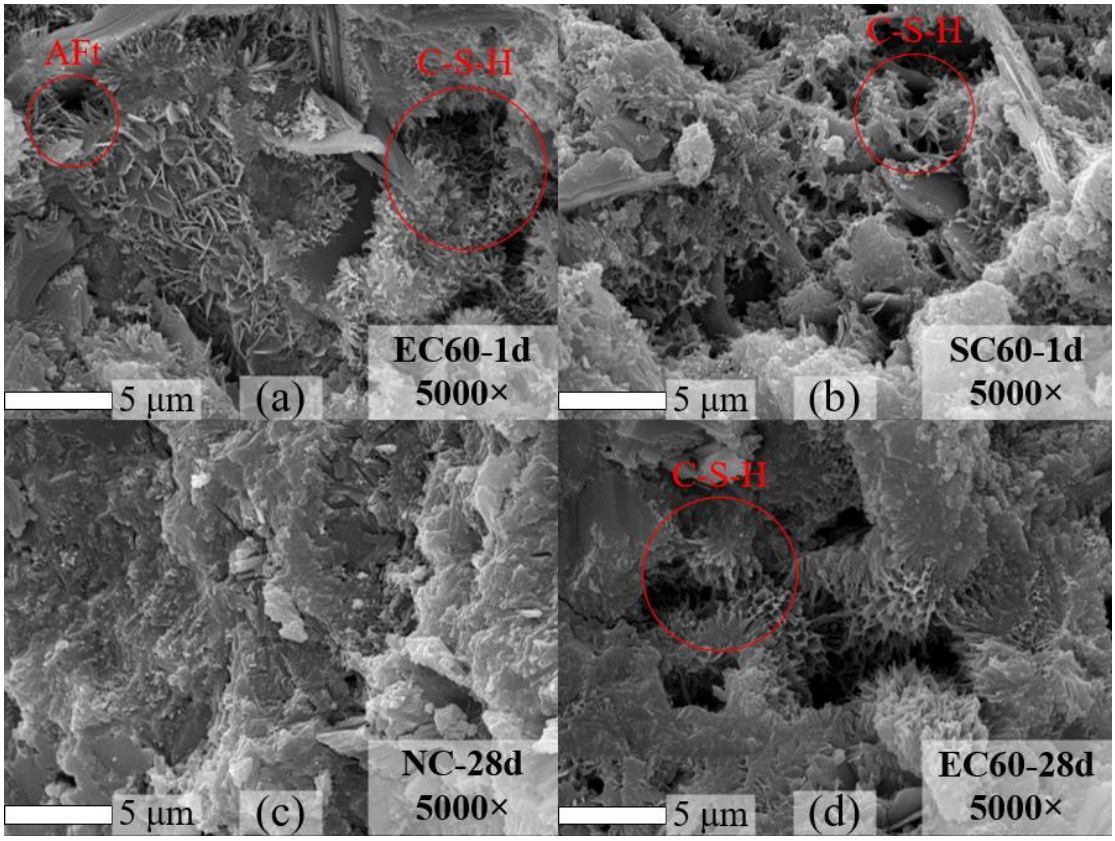

Figure 14. The 5000× SEM picture of specimens

3.4.3 Energy consumption

Based on this investigation, it can be found that EC is a curing method with easy temperature control and good curing quality. For both curing methods, energy consumption is an important criterion for judging the greening of production. In this paper, the energy consumption of SC and EC was calculated for each group of data collected from 24 4cm x 4cm x 16cm cement mortar specimens. For the EC specimens, the current and voltage values of each specimen recorded by the paperless recorder were used to calculate the total energy consumption; And the current values of the water bath tank were collected by the paperless recorder for calculation for SC specimens.

The energy consumption and power of SC and EC were calculated using the following Equation 5 and Equation 6. In order to facilitate the comparison of the energy consumption difference between the two test methods, this calculation was only used to test the energy consumption of the test equipment, which includes not limited to the hydration exothermic value of the specimen, the heat dissipation of the curing chamber to the surrounding environment, so the data was only used as semi-quantitative analysis. Energy consumed per unit area was calculated by dividing the total energy consumption by the total surface area of the specimens. The surface area of EC specimens was $24 \times 40mm \times 150mm = 0.144m^2$ due to the layout of the electrode sheet, and the surface area of SC was $24 \times 40mm \times 160mm = 0.1536m^2$. Energy consumed per kilogram was calculated by diving the total energy consumption by the total weight the specimens. The weight of EC specimens was

$$\mathrm{W} = P \times \mathrm{t} \tag{5}$$

Preprints (www.preprints.org) | NOT PEER-REVIEWED | Posted: 27 October 2021 doi:10.20944/preprints202110.0418.v1

$$P = \mathrm{U} \times \mathrm{I} \quad (6)$$

Where W was the energy consumption, P was the power, t was the time, U was the voltage (the voltage of SC specimen was 220V, EC specimens were collected by paperless recorder), I was the current recorded by the recorder. Energy consumed per unit area (kWh/m^2) was calculated by dividing the total energy consumption by the total surface area of the specimens. Energy density (kWh/kg) was calculated by diving the total energy consumption by the total weight the specimens.

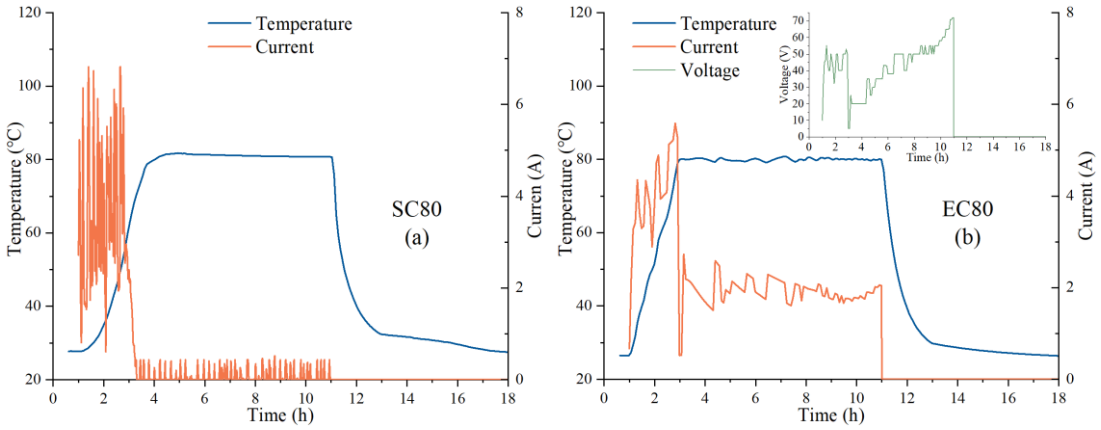

Figure 15. Current and voltage data collected during the 80℃ curing regime.

To facilitate the observation of the energy consumption of the curing regime, the most energy-consuming 80°C curing regime was plotted in Fig.15, which showed the current and voltage values collected by the paperless recorder in the 80°C curing regime. Where Fig.15(a) displayed the operated current of the water bath tank, Fig.15(b) displayed the average current values and real-time voltage values in the EC80 specimens. The results of all curing regimes calculated by Equation 5 and 6 were displayed in Tab.6.

Table 6. Energy consumption of steam curing versus direct electric curing

Curing method	Energy Consumption (kWh)	Energy consumed per unit area (kWh/m^2)	Energy density (kWh/kg)
SC80	2.35	15.28	0.162
EC80	1.03	7.18	0.076
SC60	1.83	11.93	0.126
EC60	0.59	4.10	0.043
SC40	1.51	9.83	0.104
EC40	0.16	1.14	0.012

SC consumed more energy than EC under the same curing regime, 2.28-9.44 times more than EC. The energy consumption of SC was significantly higher than that of EC under the action of the equipment used in this paper, indicating that EC is a low-energy curing method. The energy consumption per unit area of SC was 8.62, 2.91, 2.13 times higher than that of EC at 40°C, 60°C and 80°C curing regime, respectively. These results were different from the literature [17], because of this test considered a long-time temperature control curing, and the electrical or thermal energy was used to control the temperature of the specimen. In addition, the energy consumption mentioned in the literature [17] only applied the same voltage to the specimen. The resistivity of the

Preprints (www.preprints.org) | NOT PEER-REVIEWED | Posted: 27 October 2021 doi:10.20944/preprints202110.0418.v1

specimen rose sharply due to the continuation of hydration, which led to a sharp decrease in electrical power reducing energy consumption. And in order to control the temperature of the specimen, this paper promoted the Joule heat generation of the specimen with rising resistivity by increasing the voltage, which greatly consumed the electric power. This was the reason why the energy consumption per unit area in this paper was higher than that in the literature [17], which also showed that SC and EC were more energy-consuming under the long-time temperature-controlled curing regime.

The energy density of EC was similar to the results calculated in the literature [22], but the data changed due to the different time of the constant temperature period. This indicated that EC is a curing method with less energy consumption than SC, especially in the 40°C curing regime where the difference in energy consumption between the two methods could be clearly seen. The energy consumption and temperature correlation were plotted in Fig.16, demonstrating the total energy consumption for SC and EC at different curing regimes and the trend lines and correlation coefficients R^2.

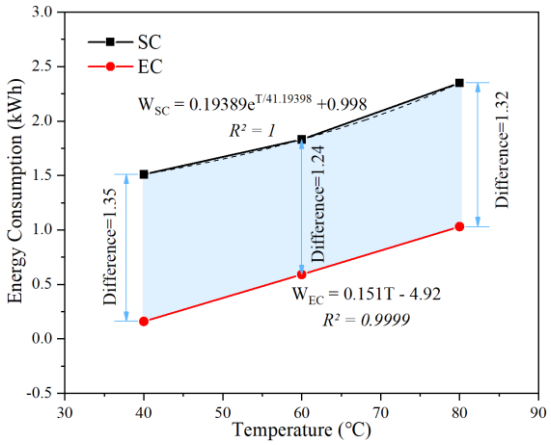

Figure 16. Correlation between energy consumption and temperature in SC and EC

The energy consumption of SC was always higher than that of EC, which was caused by the heat flow transfer characteristic of SC. The energy was first used to heat the water in the water bath tank and then to heat the specimen through the water vapor temperature, which was indirect heating. While the heat flow transfer characteristic of EC was to raise the temperature of the specimen through Joule heat, which was a direct heating and could raise the temperature of the specimen quickly and effectively. In addition, the energy consumption of SC needed to be analyzed with an exponential function, which means that as the temperature of the curing regime increases, the energy consumed would increase exponentially, unlike the linear relationship between the energy consumption of EC, which was proportional to the temperature of the specimen.

The results of the energy consumption analysis showed that EC is a lower energy consumption curing method than SC, and the directness and greenness of the volume-heating proved that EC is an excellent curing method to harden the cement-based materials quickly and improve the early mechanical properties.

Conclusion

In this paper, the effects of SC and EC on the mechanical properties and

microstructure of cement-based materials were investigated through comparative experiments. The differences in mechanical properties were explained by the hydration degree and products of the cement pastes as well as the pore structure. And the energy consumption of SC and EC regime was also analyzed. The final conclusions were obtained as follows:

1. EC achieved better mechanical properties than SC. The early properties of EC were higher than those of SC for different temperature curing regimes, and the mechanical properties of EC grew faster than those of SC with increasing age.

2. The hydration degree and hydration products in cement-based materials by SC and EC was basically the same tested by TG and XRD.

3. The pore structure of EC specimens were better than that of SC. The MIP tests showed that EC samples formed more smaller pores (Pore size less than 100nm) than SC samples and reduced the formation of large pores. The results of MIA showed that the air voids formed in the SC and EC specimens had the same distribution, but the cumulative air content of EC specimens was less than that of SC. The difference in pore structure was the main reason for the difference in mechanical properties between SC and EC.

4. EC is a volume-heating curing method while SC is a surface-heating curing method. Therefore, EC is easier to control and stabilize the temperature of the specimen in the temperature evolution during curing regime than SC. In terms of heat flow transfer characteristics, EC is easier to form a uniform temperature field in specimen than SC, which reduces the formation of temperature gradients inside the specimen.

5. EC had lower energy consumption than SC. SC consumed 2.13-8.62 times more energy than EC. In addition, the uniform heating of the specimens and the control of the specimen temperature by EC, which reduced the adverse effects on the long-term mechanical properties. Therefore, EC is a better choice for SC to produce green, low-energy, high-early-strength precast concrete elements.

References

[1] J. He, G. Long, K. Ma, Y. Xie, C. Ma, Hydration heat evolution of Portland cement paste during unsteady steam curing process: Modelling and optimization, Thermochim. Acta. 694 (2020) 178784, 10.1016/j.tca.2020.178784.

[2] C. Zou, G. Long, X. Zeng, C. Ma, Y. Xie, Z. Sun, Water evolution and hydration kinetics of cement paste under steam-curing condition based on low-field NMR method, Constr. Build. Mater. 271 (2021) 121583, 10.1016/j.conbuildmat.2020.121583.

[3] P.N. Hiremath, S.C. Yaragal, Effect of different curing regimes and durations on early strength development of reactive powder concrete, Constr. Build. Mater. 154 (2017) 72-87, 10.1016/j.conbuildmat.2017.07.181.

[4] B. Liu, J. Jiang, S. Shen, F. Zhou, J. Shi, Z. He, Effects of curing methods of concrete after steam curing on mechanical strength and permeability, Constr. Build. Mater. 256 (2020) 119441, 10.1016/j.conbuildmat.2020.119441.

[5] J. Yang, H. Hu, X. He, Y. Su, Y. Wang, H. Tan, H. Pan, Effect of steam curing on compressive strength and microstructure of high volume ultrafine fly ash cement mortar, Constr. Build. Mater.

266 (2021) 120894, 10.1016/j.conbuildmat.2020.120894.

[6] L. Chen, K. Zheng, T. Xia, G. Long, Mechanical property, sorptivity and microstructure of steam-cured concrete incorporated with the combination of metakaolin-limestone, Case Studies in Construction Materials. 11 (2019) e267, 10.1016/j.cscm.2019.e00267.

[7] C. Liu, M. Zhang, Effect of curing temperature on hydration, microstructure and ionic diffusivity of fly ash blended cement paste: A modelling study, Constr. Build. Mater. 297 (2021) 123834, 10.1016/j.conbuildmat.2021.123834.

[8] C. Zou, G. Long, X. Zeng, K. Ma, Y. Xie, Hydration and multiscale pore structure characterization of steam-cured cement paste investigated by X-ray CT, Constr. Build. Mater. 282 (2021) 122629, 10.1016/j.conbuildmat.2021.122629.

[9] C. Zou, G. Long, Y. Xie, J. He, C. Ma, X. Zeng, Evolution of multi-scale pore structure of concrete during steam-curing process, Micropor. Mesopor. Mat. 288 (2019) 109566, 10.1016/j.micromeso.2019.109566.

[10] P. Wang, H. Fu, T. Guo, W. Zuo, H. Zhao, L. Tian, C. Chen, Volume deformation of steam-cured concrete with fly ash during and after steam curing, Constr. Build. Mater. 306 (2021) 124854, 10.1016/j.conbuildmat.2021.124854.

[11] J. Shi, B. Liu, F. Zhou, S. Shen, J. Dai, R. Ji, J. Tan, Heat damage of concrete surfaces under steam curing and improvement measures, Constr. Build. Mater. 252 (2020) 119104, 10.1016/j.conbuildmat.2020.119104.

[12] Y. Yu, Z. Jin, S. Shao, X. Zhang, N. Li, C. Xiong, Evolution of temperature stress and tensile properties of concrete during steam-curing process, Constr. Build. Mater. 305 (2021) 124691, 10.1016/j.conbuildmat.2021.124691.

[13] Y. Xiang, G. Long, Y. Xie, K. Zheng, Z. He, K. Ma, X. Zeng, M. Wang, Thermal damage and its controlling methods of high-speed railway steam-cured concrete: A review, Struct. Concrete. 22 (S1) (2021) E1074-E1092, https://doi.org/10.1002/suco.202000433.

[14] J. Shi, B. Liu, F. Zhou, S. Shen, A. Guo, Y. Xie, Effect of steam curing regimes on temperature and humidity gradient, permeability and microstructure of concrete, Constr. Build. Mater. 281 (2021) 122562, 10.1016/j.conbuildmat.2021.122562.

[15] D. Cecini, S.A. Austin, S. Cavalaro, A. Palmeri, Accelerated electric curing of steel-fibre reinforced concrete, Constr. Build. Mater. 189 (2018) 192-204, 10.1016/j.conbuildmat.2018.08.183.

[16] J.G. Wilson, N.K. Gupta, Assessment of structure formation in fresh concrete by measurement of its electrical resistance: Investigation reports on accelerated curing of concrete using direct electrical conduction with a view to minimizing the temperature rise and so improving durability and reducing energy costs, Build. Res. Inf. 24 (4) (1996) 209-212.

[17] Z. Yang, Y. Xie, J. He, X. Zeng, K. Ma, G. Long, Experimental investigation on mechanical strength and microstructure of cement paste by electric curing with different voltage and frequency, Constr. Build. Mater. 299 (2021) 123615, 10.1016/j.conbuildmat.2021.123615.

[18] K.K.B.G. Bredenkamp S, Direct electric curing of concrete, Magzine of Concrete Research. 162 (45) (1993) 71-74.

[19] I.D. Kafry, Direct electrical curing of concrete: basic design, Whittles Publishing, 1999.3

[20] S. Wadhwa, L. Srivastava, D. Gautam, D. Chandra, Direct electric curing of in situ concrete, Building Research and Information - BUILDING RES INFORM. 15 (1987) 97-101, 10.1080/09613218708726799.

[21] J.G. Wilson, N.K. Gupta, Analysis of power distribution in reinforced concrete during accelerated

curing using electroheat, IEE Proceedings-Electric Power Applications. 143 (2) (1996) 172-176.

[22] J.G. Wilson, N.K. Gupta, Equipment for the investigation of the accelerated curing of concrete using direct electrical conduction, Measurement. 35 (3) (2004) 243-250, 10.1016/j.measurement.2003.11.002.

[23] C. Ma, J. Peng, H. Zhou, R. Zhou, W. Ren, Y. Du, An effective method for preparing high early-strength cement-based materials: The effects of direct electric curing on Portland cement, Journal of Building Engineering. 43 (2021) 102485, 10.1016/j.jobe.2021.102485.

[24] T. Uygunoğlu, 0. Hocaoğlu, Effect of electrical curing application on setting time of concrete with different stress intensity, Constr. Build. Mater. 162 (2018) 298-305, 10.1016/j.conbuildmat.2017.12.036.

[25] A. Susanto, G. Peng, D.A. Koleva, K. van Breugel, Electrical current flow and cement hydration: implications on cement-based microstructure, International Journal of Structural and Civil Engineering Research. 6 (2) (2017) 1-8.

[26] M. Kovtun, M. Ziolkowski, J. Shekhovtsova, E. Kearsley, Direct electric curing of alkali-activated fly ash concretes: a tool for wider utilization of fly ashes, J. Clean. Prod. 133 (2016) 220-227, 10.1016/j.jclepro.2016.05.098.[2]

[28] W. Tian, B. Qi, Y. Liu, K. Liu, W. Wang, Early frost resistance and permeability properties of carbon fiber/cement-based composite cured by ohmic heating under ultra-low temperature, Constr. Build. Mater. 282 (2021) 122729, 10.1016/j.conbuildmat.2021.122729.

[29] Y. Liu, M. Wang, W. Wang, Electric induced curing of graphene/cement-based composites for structural strength formation in deep-freeze low temperature, Materials & Design. 160 (2018) 783-793, 10.1016/j.matdes.2018.10.008.

[30] Y. Liu, M. Wang, W. Wang, Ohmic heating curing of electrically conductive carbon nanofiber/cement-based composites to avoid frost damage under severely low temperature, Composites Part A: Applied Science and Manufacturing. 115 (2018) 236-246, 10.1016/j.compositesa.2018.10.008.

[31] W. Tian, M. Wang, Y. Liu, W. Wang, Ohmic heating curing of high content fly ash blended cement-based composites towards sustainable green construction materials used in severe cold region, J. Clean. Prod. 276 (2020) 123300, 10.1016/j.jclepro.2020.123300.

[32] Y. Liu, M. Wang, W. Tian, B. Qi, Z. Lei, W. Wang, Ohmic heating curing of carbon fiber/carbon nanofiber synergistically strengthening cement-based composites as repair/reinforcement materials used in ultra-low temperature environment, Composites Part A: Applied Science and Manufacturing. 125 (2019) 105570, 10.1016/j.compositesa.2019.105570.

[33] W. Tian, Y. Liu, W. Wang, Multi-structural evolution of conductive reactive powder concrete manufactured by enhanced ohmic heating curing, Cement and Concrete Composites. 123 (2021) 104199, 10.1016/j.cemconcomp.2021.104199.

[34] Y. Liu, W. Tian, M. Wang, B. Qi, W. Wang, Rapid strength formation of on-site carbon fiber reinforced high-performance concrete cured by ohmic heating, Constr. Build. Mater. 244 (2020) 118344, 10.1016/j.conbuildmat.2020.118344.

[35] M. Jung, J. Park, S. Hong, J. Moon, Electrically cured ultra-high performance concrete (UHPC) embedded with carbon nanotubes for field casting and crack sensing, Materials & Design. 196 (2020) 109127, 10.1016/j.matdes.2020.109127.

[36] M. Wang, Y. Xie, G. Long, C. Ma, X. Zeng, F. Qiang, The impact mechanical characteristics of steam-cured concrete under different curing temperature conditions, Construction & building

materials. 241 (2020) 118042, 10.1016/j.conbuildmat.2020.118042.

[37] J. He, G. Long, C. Ma, K. Ma, Y. Xie, Y. Shi, N. Li, Z. Cheng, Effect of Triethanolamine on Hydration Kinetics of Cement – Fly Ash System at Elevated Curing Temperature, Acs Sustain. Chem. Eng. 8 (27) (2020) 10053-10064, 10.1021/acssuschemeng.0c01763.

[38] S. Jin, J. Zhang, S. Han, Fractal analysis of relation between strength and pore structure of hardened mortar, Constr. Build. Mater. 135 (2017) 1-7, 10.1016/j.conbuildmat.2016.12.152.

[39] M. Ren, X. Wen, X. Gao, Y. Liu, Thermal and mechanical properties of ultra-high performance concrete incorporated with microencapsulated phase change material, Constr. Build. Mater. 273 (2021) 121714, 10.1016/j.conbuildmat.2020.121714.